Graphene-analogues Boron Nitride nanosheets with ultrahigh ionic liquid uptake capacity as quasi-solid electrolytes

Mingtao Li[1,3†], Wenshuai Zhu[2,3†], Pengfei Zhang[3], Bolun Yang[1], Huaming Li[2], Qian He[4], Albina Borisevich[4,5] & Sheng Dai[3]

Dr. M. T. Li, Prof. B. Yang

1 Xi'an Jiaotong University, Xi'an, China

School of Chemical Engineering and Technology, Xi'an Jiaotong University, Xi'an, Shaanxi 710049, China

Dr. W. S. Zhu, Prof. H. M. Li

2 School of Chemistry and Chemical Engineering, Jiangsu University, Zhenjiang 212013, China

Dr. Q. He, Dr. A. Borisevich

4 Materials Science and Technology Division, Oak Ridge National Laboratory, Oak Ridge, Tennessee 37831, USA

Dr. A. Borisevich

5 Center for Nanophase Materials Sciences, Oak Ridge National Laboratory, Oak Ridge, Tennessee 37831, USA

Dr. M. T. Li, Dr. W. S. Zhu, Dr. P. F. Zhang, Dr. S. Dai

3 Chemical Science Division, Oak Ridge National Laboratory, Oak Ridge 37831, Tennessee, USA

[†]These authors contributed equally to this work. Correspondence and requests for materials should be addressed to W. S. Zhu. (email: zhuws@ujs.edu.cn) or to S. Dai (email: dais@ornl.gov).

Abstract: Inorganic nanoparticles are typically used as electrode materials in lithium batteries. However, to cope with the most challenge that solid electrolytes have low ionic conductivity at room

or lower temperatures, here we show graphene-analogues boron nitride (g-BN) nanosheets absorbing a large quantity of ILs as a solid-like electrolyte. The layered g-BN nanosheets have very high specific surface area, and they could absorb the IL as much as 10 times of its own weight. The ionic conductivity of the solid-like electrolyte is 3.85×10^{-3} S cm^{-1} at 25 ℃，even though at -20 ℃ it still reaches 2.32×10^{-4} S cm^{-1}, which are very close to that of the ionic liquid electrolytes. The high ionic conductivity is attributed to ordered lithium ion transport channels within g-BN nanolayers which are formed as the IL solution fills in. Furthermore, the electrolyte displays outstanding electrochemical properties and battery performance. This work opens up a new field for the application of layered nanomaterials in energy conversion devices.

Key Words: Nanolayered boron nitride, Solid electrolytes, Ionic liquids, Ionic conductivity

Solid electrolytes are the most attractive alternative to liquid carbonate-based electrolytes to improve the safety of rechargeable lithium batteries because they prevent leakage, volatilization, and flammability[1-4]. Solid electrolytes generally include inorganic and polymer solid electrolytes. In past decade, although much endeavor has been devoted to improve the ionic conductivity of those electrolytes, they still suffer from relatively poor ionic conductivity at low temperatures[5]. Another challenge in terms of the application of the solid electrolytes in lithium batteries comes from high interface resistance related to an instable contact between the solid electrolyte and the electrode. In past decade, although much endeavor has been made to address these issues, it is still difficult to acquire both high ion conductivity and a good contact between electrode/electrolyte interfaces, when only solid electrolyte materials are used in battery systems[6].

Ionic liquids (ILs) have concentrated great interest for their unique characteristics such as negligible vapor pressure, nonflammability, good thermal stability, and wide electrochemical windows[7, 8]. Incorporation of ILs into polymers or inorganic materials can effectively improve the ionic conductivity of the solid electrolytes, as well as distinctly reduce the interface resistance between the electrode and the electrolyte. Typically, polymer electrolytes consisting of lithium salt, ILs and various polymer host such as poly(ethylene oxide)[9-11], PVdF-HFP[12-14], and polymerized ionic liquids (PILs)[15-19] have been synthesized and their applications in batteries at elevated

temperatures were reported. Although ILs in these polymer electrolytes increase the ionic conductivity and decrease the electrode/electrolyte interface resistance, the ionic conductivity of them at room temperature is still low and the battery performance is not favorable, which is attributed to the discontinuous transport channels of lithium ions formed by a little amount of ILs. Recently, inorganic hybrid solid electrolytes were developed, which consisted of lithium salt, IL and SiO_2 or TiO_2 nanoparticles[20-22]. The nanoparticles can provide an effective pathway for the transport of lithium ions by their self-arrangement. Hence, the ionic conductivity at room temperature and the interface compatibility between the electrolytes and electrodes improve obviously. However, restricted to smaller specific surface area, the amount of IL encapsulated by the nanoparticles is limited.

Graphene-analogue boron nitride (g-BN) nanosheets have drawn much attention due to their remarkable properties[23-24], such as a wide energy band gap[25], high thermal conductivity[26], good chemical stability[27], high surface area[28, 29] and excellent adsorption performance[30-32]. On account of its high specific surface area and special interlayer structure, the g-BN nanosheets could remain solid phase even if they absorb the ten-fold mass equivalent of ILs[33]. More importantly, the special layer structure of the IL confined between the g-BN nanosheets leads to the formation of continuous transport channels for lithium ions, greatly increasing the ionic conductivity. Moreover, the ultrahigh ionic-liquid uptake capacity of g-BN results in low interface resistance due to the stable contact between the solid electrolyte and electrodes.

Inspired by that concept, in this work the few-layered g-BN with a highly abundant nanoporous structure is developed as an electrolyte host. A solid-like electrolyte is designed by which the g-BN nanosheet absorbs a large quantity of ILs. The solid-like electrolyte displays not only the exceptional ionic conductivity (more than 10^{-3} S cm^{-1}) at room temperature but also the low interface resistance and improved interface compatibility. Furthermore, batteries derived from the above quasi-solid electrolyte display a high capacity and good cycling stability.

Results

Synthesis and characterization of g-BN.

We explored a synthesis route of porous BN nanosheets depending on a template-free method, as illustrated in Scheme 1. The mixture of boron oxide (B_2O_3) and urea (CON_2H_4) in ethanol aqueous

was recrystallized. Then the obtained mixture was heated gradually in tube furnace under nitrogen. Based on the intricate urea pyrolysis procedure[34], we propose the formation process of few-layered nanoporous g-BN (see Supplementary Scheme S1). When the temperature was raised to 200℃, urea transferred to liquid and polycondensated to the intermediate cyanuric acid $(C_3H_3N_3O_3)$[35]. Urea melted into liquid, functionalizing not only as solvothermal solvent to promote the molecular diffusion but as the peeling role to control formation of few-layered g-BN.[36, 37] Increasing the temperature continuously, g-BN grows up. During this process, urea and formed urea intermediates decomposed to NH_3, CO_2 and H_2O bubbles which play a pores-creating role for the resultant nanoporous structure. Finally, few-layered and nanoporous g-BN could be fabricated.
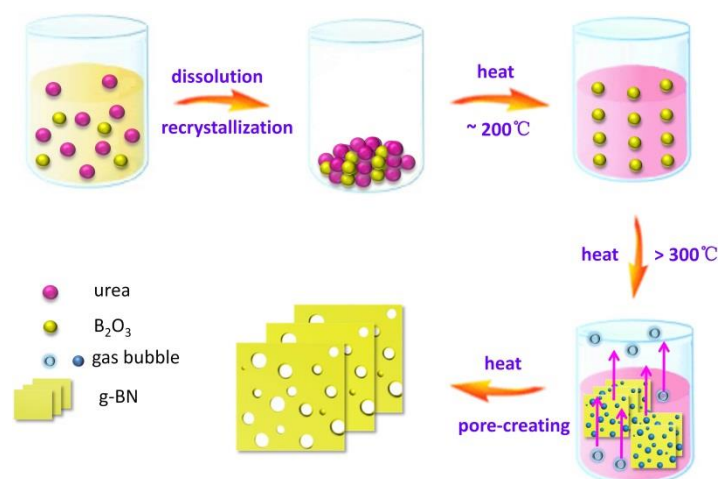
Scheme 1 ｜Schematic of the synthesis process of g-BN

The g-BN nanosheets with porous structure have been verified by a BET measurement. Figure 1a) and 1b) indicate nitrogen isotherms and pore size distribution curves of the nanosheets, which can be categorized as type II based on the IUPAC classification, and type H3 hysteresis loop in the relative pressure range of 0.45–1.0 indicates the presence of nanosheets materials.[38] Additionally, very Low pressure adsorption presents a micropore-filling behavior. Moreover, the type H3 hysteresis loop at a relative pressure of 0.45 to 1.0 suggests the presence of slits-shaped pores, in line with the shape of the sheet-like nanostructures. The total BET surface area, micropore surface area, micropore volume, and pore diameter of the g-BN, which are 860 $m^2 \cdot g^{-1}$, 602 $m^2 \cdot g^{-1}$, 0.2 $cm^3 \cdot g^{-1}$ and 2 nm, respectively (Supplementary Table S1). High surface area and the surface micropore nanostructure contribute to high adsorptive capability for the IL solution. The g-BN nanosheets can adsorb ten-fold Li-IL to form a solid-like electrolyte.
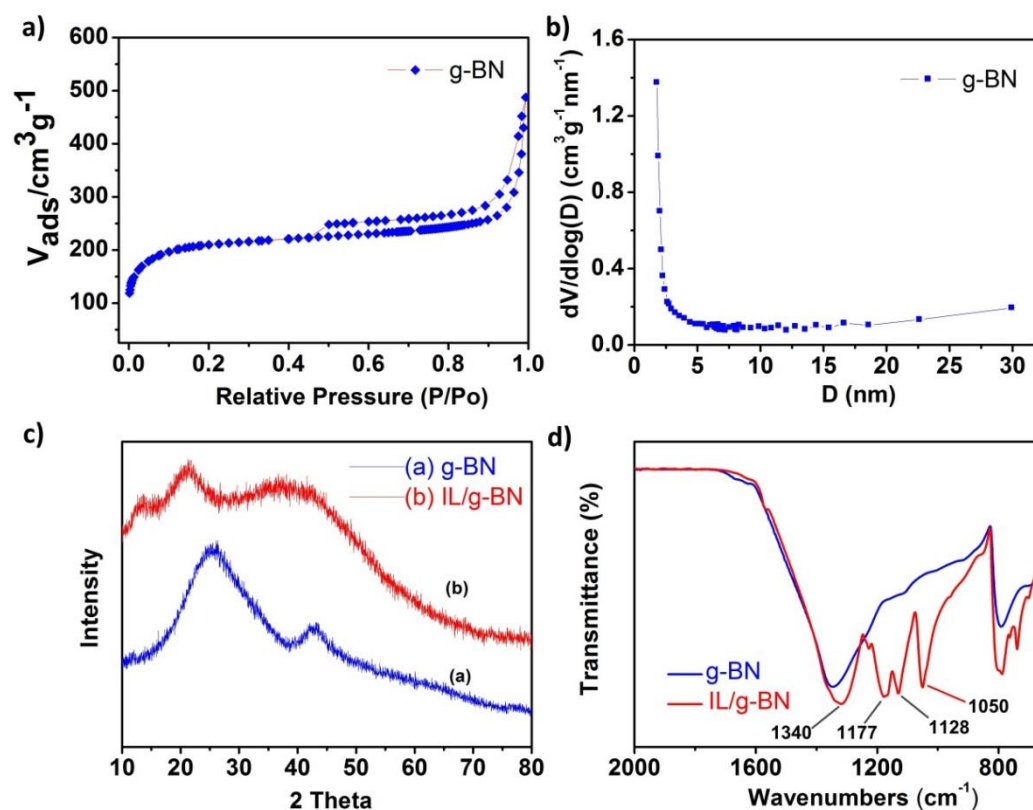
Figure 1 | **Structure and surface property of g-BN. a)** N_2-sorption isotherms of g-BN. **b)** BJH pore size distribution. **c)** XRD patterns of g-BN and Li-IL/g-BN. **d)** FT-IR spectra of g-BN and Li-IL/g-BN.

The XRD patterns of both g-BN and g-BN-supported Li-IL solid-like electrolyte are shown in Figure 1c. The two peaks corresponding to the (002) and (100) planes of g-BN are readily in accordance with the standard hexagonal phase of h-BN (JCPDS Card No. 34-0421), demonstrating that the as-obtained g-BN has a hexagonal structure.[26] When the g-BN adsorbs Li-IL, an obvious shift from 2θ=24° to low angles can be observed, indicating that Li-IL may embed the inter-layer space of the g-BN.[38] Hence, the increase of inter-distance between the (002) basal planes may be responsible for the intercalation of the Li-IL in the inter-layer space. The g-BN absorbing with Li-IL was further determined by FT-IR spectrum in Fig. 1d). In the case of g-BN, the absorption band centered around 1360 cm^{-1} and 795 cm^{-1} can be attributed to the in-plane B-N transverse optional mode and out-of-plane B-N-B bending mode of hexagonal boron nitride.[39] After absorbing Li-IL, four peaks in the appeared (1340, 1177, 1128, and 1050 cm^{-1}) that could be assigned to the vibration sorption of TFSI anions of ILs (v_a(SO$_2$), v_a(CF$_3$), v_s(SO$_2$), and v_a(S-N-S)[40], respectively.

In order to further investigate the formation of continuous transport channels of lithium ions, the

microscopic performance of the g-BN and solid electrolyte samples were used to determine. From the SEM images (Supplementary Figure S1), the nanosheets of the g-BN can be clearly observed, and after absorbing the Li-IL solution they still exist around the groups of nanosheets of the g-BN. The lower magnification STEM images in Figure 2*(a)* and 2*(d)* also verify that g-BN maintained a graphene-like flake morphology after the absorption of IL. Higher magnification images in Figure 2*(b)* and 2*(e)* further reveal the polycrystalline feature of the g-BN with few-layers structure (3~4 layers). Moreover, the hexagonal structure of g-BN (Fig. 2c and 2f) can also be seen clearly from the lattice fringes. After absorbing the IL solution, the g-BN nanosheets supported with Li-IL still remain graphene-like layered structure (Fig. 2e) and the width of polycrystalline fringe increases compared to the g-BN (Fig. 2e), indicating the distance of nanolayers is wider due to the insertion of ILs, which is in accordance with the XRD results. Furthermore, it is also seen the IL solution disperse on the surface of the g-BN, and thus the transport channel for lithium ions in interlayer and out-of-layer can be developed. Scheme 2 illustrates the fabrication of the quasi-solid electrolytes (SE) and the pathway for lithium ion transport formed by the IL solution in the interlayer and out-of-layer of g-BN. The continuous transport channels are favorable for the fast-transport of lithium ions and may result in the high ionic conductivity.

Figure 2 ∣ **Representative STEM bright field (BF) images**. **(a-c)** g-BN and **(d-f)** 2-fold IL/g-BN samples. Lower magnification images in *(a)* and *(d)* shows that BN maintained a flake morphology after the absorption of ionic liquid. Higher magnification images *(b)* and *(e)* reveal the layer structure at the edges of the flakes, where the materials appeal to be curved into edge-on condition (white arrows). The EELS spectrum of the 2-fold IL/g-BN specimen was overlayed with *(d)* showing the B and N K-edges. The C K edge comes from the hydrocarbon contamination. These images also reveal the poly-crystalline nature of the material. The hexagonal BN structures for both materials can be seen from the lattice fringes shown in *(c)* and *(f)*.
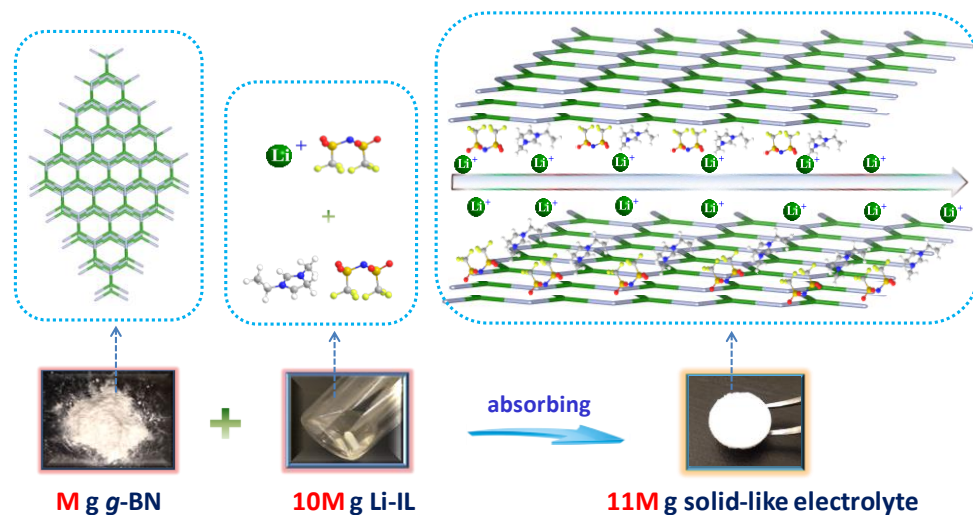
Scheme 2 | **SE pathway for lithium ion transport formed by the IL solution in the interlayer and out-of-layer of g-BN**

Measurement of electrochemical properties. To verify the above hypothesis, the ionic conductivity at different temperatures has been characterized. Figure.3a) shows the result of ionic conductivity for the SE and the Li-IL electrolyte control. The plot of SE electrolyte as the same with the Li-IL electrolyte exhibits the Vogel-Tamman-Fulcher (VTF)-type temperature dependence, which indicates the value of ionic conductivity of SE correlates with the viscosity of the solution and the hopping species in SE are determined by the property of Li-IL electrolyte[41]. It should be noted the ionic conductivity of SE is very high at room temperature that reaches 3.85×10^{-3} S cm^{-1}, even though at -20 ℃ it still is 2.32×10^{-4} S cm^{-1}. The high ionic conductivity is attributed to ordered lithium ion transport channels in g-BN nanolayers which are formed when the Li-IL fills in, as observed by STEM. The outstanding property of SE at lower temperatures opens a promising perspective as a new solid-like electrolyte in application to low temperatures for lithium batteries.
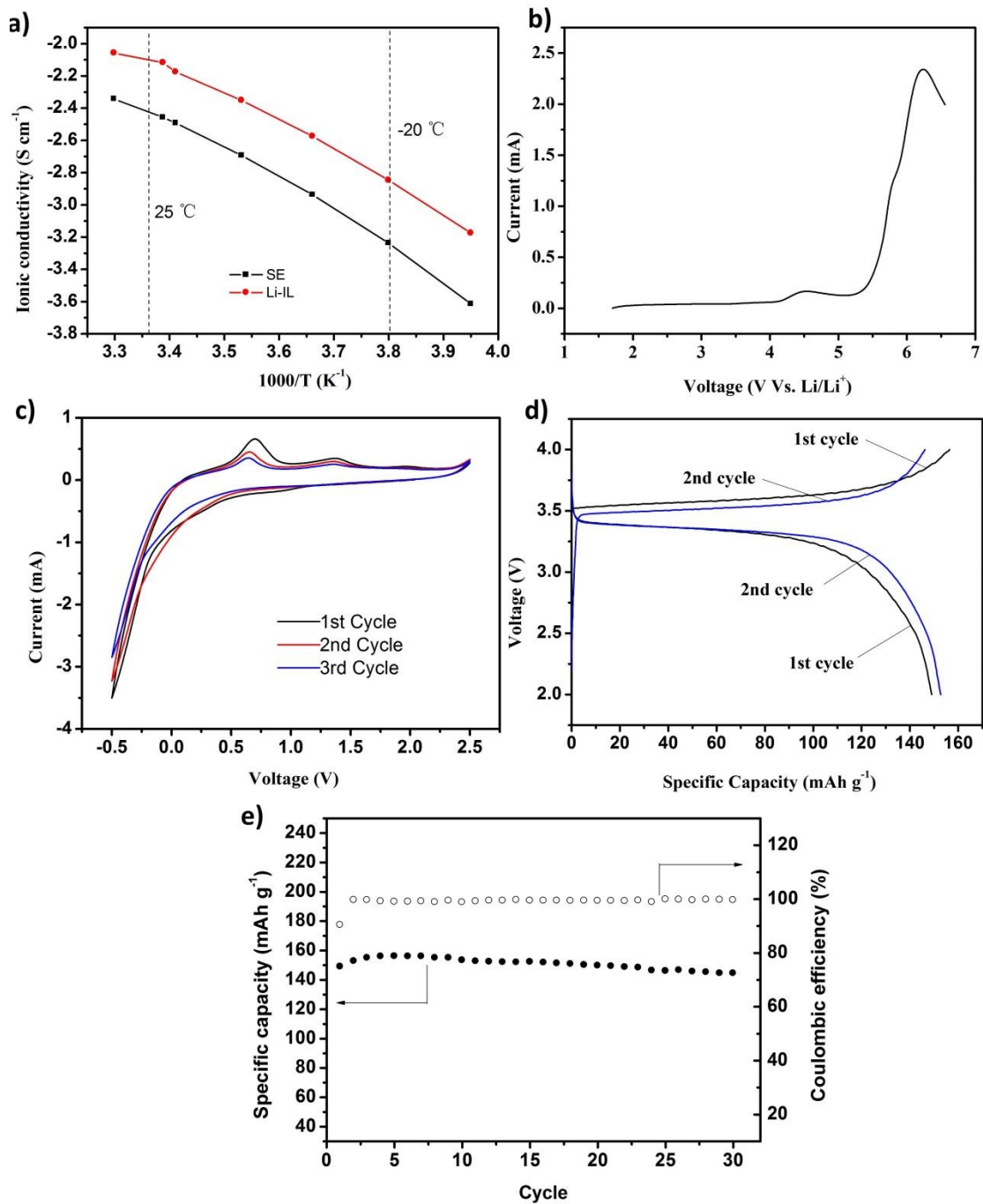
Figure 3 | Electrochemical performance of SE. a) The temperature dependence of ionic conductivity for the SE and Li-IL electrolytes. **b)** The linear sweep voltammetry curve with a Li/SE/SS cell at room temperature SS: stainless steel. **c)** Cyclic voltammograms with a Li/SE/Pt cell. Working electrode: Pt; counter electrode and reference electrode: lithium; scan rate: 10 mV s^{-1}. **d)** Voltage vs. discharge capacity profile of a Li/SE/LiFePO$_4$ cell. **e)** Discharge capacity as a function of cycle number for a Li/SE/LiFePO$_4$ cell. Charge–discharge current rate is 0.1 C.

The electrochemical stability is an important index which determines the availability of electrolytes. The electrochemical stability of the SE electrolyte was characterized by linear sweep

voltammetry with a Li/SE/SS cell at room temperature, as shown in Fig. 3b). In Fig.3b), a peak appears at about 4.5 V versus Li/Li which is associated with the oxidation decomposition of immidazolium cations in the IL. The oxidation stability of the SE electrolyte agrees with that of the IL, which is 4.3 V (corresponding to a current density of 10 mA cm^{-2}). This result demonstrates that the electrolyte has good electrochemical stability, thus confirming its feasibility for application in Li/LiFePO$_4$ batteries.

Lithium redox in the SE electrolyte was characterized by cyclic voltammograms (CVs) with a Li/SE/Pt cell, as shown in Fig. 3c). The plating of lithium on the nickel electrode could be clearly observed like EMI-TFSI IL electrolytes [42, 43]. In the first cycle for the SE electrolyte, the cathodic peak corresponding to the plating of lithium is about -0.12 V vs. Li/Li$^+$, and in the returning scan the anodic peak corresponding to the stripping of lithium is around 0.15 V vs. Li/Li$^+$. It is noteworthy that in case of the Pt electrode, the peak at 0.7 V vs. Li/Li$^+$ due to the formation of a Li-Pt alloy could be clearly observed[44]. The lithium redox in the SE electrolyte could be generated by forming a certain surface film (SEI) on the Pt electrode. The redox peak currents decrease gradually with the cycle numbers. This suggests that the SEI film turns thicker and thicker so that the lithium reduction and oxidation is restrained gradually.

The charge–discharge performance of Li/SE/LiFePO$_4$ batteries was characterized at room temperature, and their cycling properties are presented in Fig. 3e. The discharge capacity and the coulombic efficiency of the battery are found to be 149 mAh g^{-1} and 90.5% in the first cycle, respectively. During the initial 4 cycles, the discharge capacity and the culombic efficiency increased gradually, perhaps as a result of generation of improved penetration and contact of the IL component from the electrolyte into the electrode material. After an increasing step, the cell delivers a maximum capacity of about 155 mAh g^{-1}, and the culombic efficiency reaches 99%. Subsequently, the battery capacity decreases slowly during cycling. It is found that the battery performance is greatly associated with the thickness of the solid-like electrolyte membrane and the shaping stress of the membrane. The optimizing technology of the fabrication for SE membranes is ongoing.

Discussion

The g-BN nanosheets have high specific surface area which is attributed to its poly-crystalline nature and few-layer structure. When the small amount of Li-IL is supported on g-BN, the Li-IL

could cover the outside surface of the nanolayers. As the amount of the Li-IL increases, the Li-IL gradually enter the inter-layer space of g-BN, which is demonstrated by XRD patterns for different contents of the Li-IL showed in Figure 4. The (002) diffraction peak hardly shift when the content of the Li-IL is less than 0.4-fold of the weight ratio of g-BN, and afterwards a clear shift of the (002) diffraction peak to low angles is observed and the intensity of the peaks increases obviously as the content of the Li-IL increases, which verified the distance between the (002) basal planes is broadened. Thus, it could be inferred the pathway for lithium ions transport in SE consists of two parts, the outside surface space and the inter-layer space of g-BN.
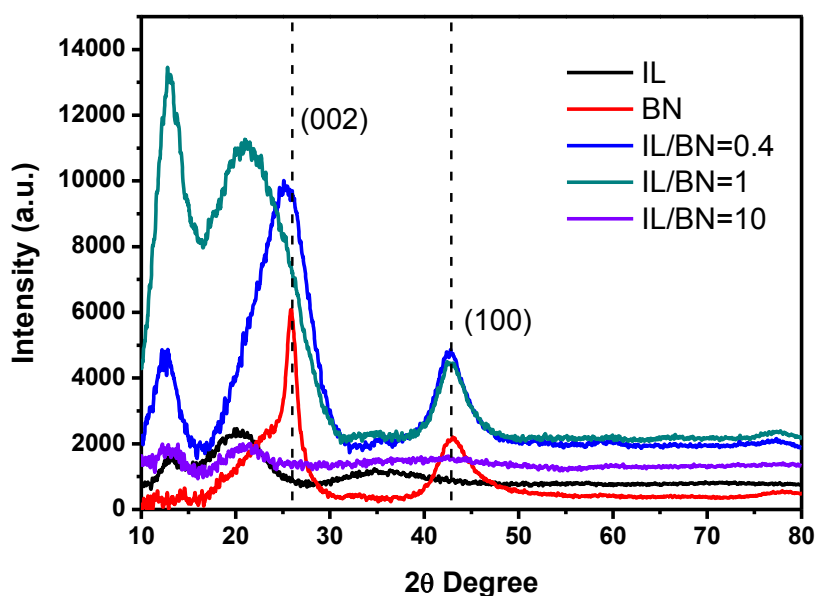

Figure 4 | XRD patterns for different contents of the Li-IL in g-BN nanosheets

Additionally, the content of ILs greatly affects the electrochemical performance of the SE. From the Supplementary Figure S3, the temperature dependence of ionic conductivity for the different contents of the SE, we can know the ionic conductivity increases apparently as the content of ILs, and it more and more approaches the value of the IL electrolyte. Another advantage of increasing the IL solution is that the interface resistance between the SE and electrodes decreases and the interface compatibility improves, as the content of ILs increases.

In conclusion, graphene-analogues g-BN nanosheets have been synthesized using a thermal treatment process without utilization of any catalyst and ex situ template. The obtained g-BN nanosheets have a very high specific surface area, and they could absorb the IL solution as much as

10-fold of its own weight. The quasi-solid electrolyte has excellent ionic conductivity at room and lower temperature, and it is 3.85×10^{-3} S cm^{-1} at 25 ℃ and 2.32×10^{-4} S cm^{-1} at -20 ℃. The distinguished property of SE at lower temperatures opens a promising perspective as a new solid-like electrolyte in application to low temperatures for lithium batteries. The high ionic conductivity is resulted from ordered lithium ion transport pathways between g-BN nanolayers which are developed as the IL solution fills in. This work explores a new field for the application of layered nanomaterials as electrolyte host in energy conversion devices.

Methods

Materials synthesis.

Preparation of g-BN: 1.64 g boron oxide (B_2O_3) and 24 g urea(CON_2H_4) were dissolved in mixture of 40 mL ethanol and 20 mL ultra-pure water. The solution was stirred and heated at 70 ℃ until the solvent was boiled away. Then the white solid was transferred to a tube furnace, and heated to 900℃ at a heating rate of 4℃/min under N_2 atmosphere. After the temperature reached 900℃, the tube furnace was kept for another 2 h. Then, the tube furnace freely cooled to room temperature，and finally the g-BN product was obtained.[25]

The ionic liquid, EMI-TFSI was prepared according to a reference method[45]. A lithium salt-ionic liquid solution of molality 0.5 mol kg^{-1} (Li-IL) was prepared by adding a proper amount of LiTFSI to the ionic liquid. The water content of EMI-TFSI was measured by coulometric Karl Fischer titration to be 20 ppm.

Solid-like electrolytes were prepared by g-BN and the Li-IL mixed simply with the weight ratio of 1:10 in argon atmosphere, noted as SE. The ratio in the electrolyte has been optimized so as to obtain Li-IL as much as possible. This sample was used during all the electrochemical tests except battery performance.

Materials characterization.

X-ray diffraction patterns of the samples were collected using a Panalytical X'Pert PRO diffraction system with a Cu Kα radiation. Scanning electron microscopy (SEM) was performed by a Zeiss Supra 55 VP SEM. Nitrogen adsorption and desorption isotherms were obtained using a Tristar 3000 apparatus

at 77K. FTIR spectra were obtained with a Nicolet 7199 FTIR spectrometer. The specimen for electron microscopy was prepared by grinding and dispersing dry powders of the material onto 400 mesh holey carbon copper grid. The Scanning transmission electron microscopy (STEM) image was performed on Nion UltraSTEM 100 (operated at 100kV) in Oak Ridge National Laboratory.

Electrochemical measurements.

The ionic conductivity of the gel polymer electrolytes were determined from the impedance spectrum using a blocking cell of which the electrolyte was sandwiched between two stainless steel electrodes in a Swagelok cell. Electrochemical impedance spectrum measurements were performed using a VMP3 (BioLogic) over a frequency range of 1 MHz to 100 mHz with a potentiostatic signal amplitude of 10 mV. Linear sweep voltammetry (LSV) was performed at 25 ℃ (scan rate 10 mV s^{-1}) using a Pt/Solid-like electrolyte/Li Swagelok cell.

Battery test.

Lithium foil (battery grade) was used as a negative electrode. And the positive electrode was fabricated by spreading the mixture of LiFePO$_4$, acetylene black and PVdF (initially dissolved in N-methyl-2-pyrrolidone) with a weight ratio of 8:1:1 onto Al current collector (battery use). Loading of active material was about 2.0 mg cm^{-2} corresponding to 0.3 mAh cm^{-2} and this thinner electrode was directly used without pressing.

The solid-like electrolyte used in batteries was fabricated by a squash technique. g-BN and Li-IL with a weight ratio of 1:5 were dispersed in ethanol for 8 h. Then the solvent was removed at 80 ℃, and the obtained white powder was pressed into pellets with the diameter of 12 mm and the thicknesses of 0.35 mm. The as-prepared pellets were dried at 110 ℃ under vacuum for 24 h.

Li/LiFePO$_4$ polymer batteries were fabricated (in an argon-filled glove box) by laminating the lithium foil, the solid-like electrolyte and a LiFePO$_4$ cathode tape in a button cell.

Preliminary cycling tests on Li/LiFePO$_4$ polymer batteries were performed at 25 ℃ using a CT2001A cell test instrument (LAND Electronic Co., Ltd.). The charge and discharge current rates were fixed to C/10. The voltage cut-offs were fixed at 4.0 (charge step) and 2.0 V (discharge step), respectively.

Author contributions

M.T.L. and W.S.Z. contributed equally to this work. S.D., M.T.L. and W.S.Z. conceived the idea. W.S.Z. carried out the BN synthesis and characterization. M.T.L. prepared the solid-like electrolytes and performed the electrochemical test. P.F.Z., B.L.Y. and H.M.L. analyzed the physicochemical properties of this new electrolyte. Q.H. and A.B performed the STEM measurement and data analysis. M.T.L. and W.S.Z. wrote the paper. M.T.L., W.S.Z., P.F.Z. and S.D. discussed the results and participated in the preparation of the paper.

References

1. Kamaya, N. *et al.* A lithium superionic conductor. *Nat. Mater.* **10,** 682-686 (2011).

2. Lu, Y., Das, S. K., Moganty, S. S. & Archer, L. A. Ionic liquid-nanoparticle hybrid electrolytes and their application in secondary lithium-metal batteries. *Adv. Mater.* **24**, 4430-4435 (2012).

3. Srivastava, S., Schaefer, J. L., Yang, Z., Tu, Z. & Archer, L. A. 25th anniversary article: polymer–particle composites: phase stability and applications in electrochemical energy storage. *Adv.Mater.* **26**, 201-234 (2014).

4. Khurana, R., Schaefer, J. L., Archer, L. A. & Coates, G. W. Suppression of lithium dendrite growth using cross-linked polyethylene/poly(ethylene oxide) electrolytes: a new approach for practical lithium-metal polymer batteries. *J. Am. Chem. Soc*. **136**, 7395-7402 (2014).

5. Wiers, B. M., Foo, M. L., Balsara, N. P. & Long, J. R. A solid lithium electrolyte via addition

of lithium isopropoxide to a metal–organic framework with open metal sites. *J. Am. Chem. Soc.* **133**, 14522-14525 (2011).

6.   Kim, J. K., Scheers, J., Park, T. J. & Kim, Y. Superior ion-conducting hybrid solid electrolyte for all-solid-state batteries. *ChemSusChem* **8**, 636-641 (2015).

7.   Lewandowski, A. & Świderska-Mocek A. Ionic liquids as electrolytes for Li-ion batteries—An overview of electrochemical studies. *J. Power Sources* **194,** 601-609 (2009).

8.   Chai, M. *et. al.* Ether-functionalized pyrazolium ionic liquids as new electrolytes for lithium battery. *Electrochim. Acta.* **66,** 67-74 (2012).

9.   Shin, J. H., Henderson, W. A., Scaccia, S., Prosini, P. P. & Passerini, S. Solid-state Li/LiFePO$_4$ polymer electrolyte batteries incorporating an ionic liquid cycled at 40°C. *J. Power Sources* **156**, 560-566 (2006).

10.   Choi, J. *et al.* Poly(ethylene oxide)-based polymer electrolyte incorporating room-temperature ionic liquid for lithium batteries. *Solid State Ionics* **178**, 1235-1241 (2007).

11.   Cheng, H., Zhu, C., Huang, B., Lu, M. & Yang, Y. Synthesis and electrochemical characterization of PEO-based polymer electrolytes with room temperature ionic liquids. *Electrochim. Acta* **52**, 5789-5794 (2007).

12.   Ferrari, S. *et al.* Lithium ion conducting PVdF-HFP composite gel electrolytes based on N-methoxyethyl-N-methylpyrrolidinium bis(trifluoromethanesulfonyl)-imide ionic liquid. *J. Power Sources* **195**, 559-566, (2010).

13.   Kim, J. K. *et. al..* Preparation and electrochemical characterization of electrospun, microporous membrane-based composite polymer electrolytes for lithium batteries. *J. Power Sources* **178**, 815-820 (2008).

14.   Li, M. *et al.* Li/LiFePO4 batteries with gel polymer electrolytes incorporating a guanidinium-based ionic liquid cycled at room temperature and 50°C. *J. Power Sources* **196**, 6502-6506 (2011).

15.   Pont, A. L., Marcilla, R., De Meatza, I., Grande, H. & Mecerreyes, D. Pyrrolidinium-based polymeric ionic liquids as mechanically and electrochemically stable polymer electrolytes. *J. Power Sources* **188**, 558-563 (2009).

16.   Li, M., Wang, L., Yang, B., Du, T. & Zhang, Y. Facile preparation of polymer electrolytes based on the polymerized ionic liquid poly((4-vinylbenzyl)trimethylammonium bis

(trifluoromethanesulfonylimide)) for lithium secondary batteries. *Electrochim. Acta* **123,** 296-302 (2014).

17. Li, M. *et. al.* Polymer electrolytes containing guanidinium-based polymeric ionic liquids for rechargeable lithium batteries. *J. Power Sources* **196**, 8662-8668 (2011).

18. Li, M. *et al.* New polymerized ionic liquid (PIL) gel electrolyte membranes based on tetraalkylammonium cations for lithium ion batteries. *J. Membrane Sci* **447,** 222-227 (2013).

19. Yin, K. *et al.* Polymer electrolytes based on dicationic polymeric ionic liquids: application in lithium metal batteries. *J. Mater. Chem. A* **3:** 170-178 (2015).

20. Zhang, J. *et al.* Superior conductive solid-like electrolytes: nanoconfining liquids within the hollow structures. *Nano letters* **15**, 3398-3402 (2015).

21. Li, X. *et al.* Mesoporous silica/ionic liquid quasi-solid-state electrolytes and their application in lithium metal batteries. *J. Power Sources* **278,** 128-132 (2015).

22. Jung, Y. C., Lee, S. M., Choi, J. H., Jang, S. S. & Kim, D. W. All solid-state lithium batteries assembled with hybrid solid electrolytes. *J. Electrochem. Soc.* **162**, A704-A710 (2015).

23. Golberg, D. *et al.* Boron nitride nanotubes and nanosheets. *Acs Nano* **4**, 2979-2993 (2010).

24. Dean, C. R. *et al.* Boron nitride substrates for high-quality graphene electronics. *Nat. Nanotech.* **5**, 722-726 (2010).

25. Nag, A. *et al.* Graphene Analogues of BN: Novel Synthesis and Properties. *Acs Nano* **4**, 1539-1544 (2010).

26. Zhi, C. Y., Bando, Y., Tang, C. C., Kuwahara, H. & Golberg, D. Large-scale fabrication of boron nitride nanosheets and their utilization in polymeric composites with improved thermal and mechanical properties. *Adv. Mater.* **21**, 2889- 2893 (2009).

27. Song, L. *et al.* Large scale growth and characterization of atomic hexagonal boron nitride layers. *Nano Lett.* **10**, 3209-3215 (2010).

28. Weng, Q. H., Wang, X. B., Bando, Y. & Golberg, D. One-step template-free synthesis of highly porous boron nitride microsponges for hydrogen storage. *Adv. Energy Mater.* **4**, 1301525 (2014).

29. Weng, Q., Wang, X., Zhi, C., Bando, Y. & Golberg, D. Boron nitride porous microbelts for hydrogen storage. *Acs Nano* **7**, 1558-1565 (2013).

30. Liu, F., Yu, J., Ji, X. X. & Qian, M. Q. Nanosheet-structured boron nitride spheres with a versatile adsorption capacity for water cleaning. *Acs Appl. Mater. Inter.* **7**, 1824-1832 (2015).

31.   Lei, W. W., Liu, D. & Chen, Y. Highly Crumpled boron nitride nanosheets as adsorbents: scalable solvent-less production. *Adv. Mater. Interf.* **2**, 1400529 (2015).

32.   Xiong, J. et al. Graphene-like boron nitride induced remarkable adsorption capacity for dibenzothiophene in fuels, *Green Chem.* 17, 1647–1656 (2015).

33.   Zhu, W. S. *et al.* Graphene-analogue hexagonal bn supported with tungsten-based ionic liquid for oxidative desulfurization of fuels. *Acs Sustain. Chem. Eng.* **3**, 186-194 (2015).

34.   Schaber, P.A. *et al.* Thermal decomposition (pyrolysis) of urea in an open reaction vessel. *Thermochim. Acta* **424**, 131-142 (2004).

35.   Wu, P. W. *et. al.* Controllable fabrication of graphene-analogy boron nitride confined tungsten oxide nanoparticles as efficient desulfurization catalyst. *Chem. Eur. J.* DOI: 10.1002/chem. 201501413 (2015).

36.   Zhang, J. S., Zhang, M. W., Zhang, G. G. & Wang X. C. Synthesis of carbon nitride semiconductors in sulfur flux for water photoredox catalysis. *Acs Catal*. **2**, 940-948 (2012).

37.   Lee, S. C., Lintang, H. O. & Yuliati, L. A urea precursor to synthesize carbon nitride with mesoporosity for enhanced activity in the photocatalytic removal of phenol. *Chem. Asian J.* **7**, 2139-2144 (2012).

38.   Lei, W. W., Portehault, D., Liu, D., Qin, S. & Chen Y. Porous boron nitride nanosheets for effective water cleaning. *Nat. Commun.* **4**, 1777 (2013).

39.   Wang, X. B. *et al.* "Chemical blowing" of thin-walled bubbles: high-throughput fabrication of large-area, few-layered BN and C-x-BN nanosheets. *Adv. Mater.* **23**, 4072-4076 (2011).

40.   Umebayashi, Y. *et al.* Lithium ion solvation in room-temperature ionic liquids involving bis(trifluoromethanesulfonyl) imide anion studied by raman spectroscopy and DFT calculations. *J. Phys. Chem. B* **111**, 13028-13032 (2007).

41.   Suo, L., Hu, Y. S., Li, H., Armand, M. & Chen L. A new class of Solvent-in-Salt electrolyte for high-energy rechargeable metallic lithium batteries. *Nat. commun.* **4,** 1481 (2013).

42.   Sato, T., Masuda, G. & Takagi, K. Electrochemical properties of novel ionic liquids for electric double layer capacitor applications. *Electrochim. Acta* **49**, 3603-3611 (2004).

43.   Wibowo, R., Ward Jones, S. E. & Compton, R. G. Kinetic and thermodynamic parameters of the Li/Li^{+} couple in the room temperature ionic liquid N-butyl-N-methylpyrrolidinium bis(trifluoromethylsulfonyl) imide in the temperature range 298−318 K: A theoretical and

experimental study using Pt and Ni electrodes. *J. Phys. Chem. B* **113**, 12293-12298 (2009).

44. Matsumoto, H., Sakaebe, H. & Tatsumi, K. Preparation of room temperature ionic liquids based on aliphatic onium cations and asymmetric amide anions and their electrochemical properties as a lithium battery electrolyte. *J. Power Sources* **146**, 45-50 (2005).

45. Seki, S. *et al.* Lithium secondary batteries using modified-imidazolium room-temperature ionic liquid. *J. Phys. Chem. B* **110**, 10228-10230 (2006).

Additional information